High-Field Electron Mobility Model for Strained-Silicon Devices

Siddhartha Dhar, *Student Member, IEEE*, Hans Kosina, *Member, IEEE*, Gerhard Karlowatz, Stephan Enzo Ungersboeck, Tibor Grasser, *Senior Member, IEEE*, and Siegfried Selberherr, *Fellow, IEEE*

***Abstract*—The application of mechanical stress to enhance the carrier mobility in silicon has been well established in the last few years. This paper probes into the electron conduction in biaxially and uniaxially stressed silicon in the nonlinear transport regime. The electron behavior has been analyzed for different field directions and stress/strain conditions using full-band Monte Carlo simulations. An analytical model describing the velocity components parallel and perpendicular to the electric field has been developed. The model includes the effect of strain induced valley splitting and can be applied for arbitrary directions of the electric field. The extension to different field directions has been performed using a Fourier series interpolation and a spherical harmonics interpolation for transport in two and three dimensions, respectively. The model can be implemented in a drift-diffusion-based device simulator.**

***Index Terms*—Device simulation, full-band Monte Carlo simulation, high-field electron mobility, strained-silicon, technology computer-aided design (TCAD).**

I. Introduction

Uniaxially stressed silicon, offering larger electron and hole mobilities [1], [2] compared to conventional silicon is becoming increasingly accepted by the semiconductor manufacturing industry. Stress causes a deviation of the silicon lattice constant from its equilibrium value, thereby modifying the electronic band structure. Mechanical stress in silicon can be generated either globally, by growing an epitaxial layer on a relaxed SiGe substrate [3]–[5], by mechanical deformation [6], [7], or induced during the processing steps [2], [8]. Biaxially strained-silicon layers grown on relaxed SiGe substrates have shown large enhancements of electron mobility. This method however suffers from several integration issues. There has thus been a growing interest in uniaxially strained-silicon, which delivers superior mobilities for both electrons and holes.

Strain induced enhancement of the low-field electron mobility can be attributed to two concurring effects. First, intervalley phonon scattering is reduced due to a decreased number of final available states. Second, due to the energy lowering of the Δ_2 valleys, the electrons prefer to occupy this valley and therefore experience a lower in-plane conductivity effective mass. While biaxial tensile strain delivers an energy splitting of around 60 meV per 10% Ge content, uniaxial stress results in around 90 meV of splitting per 1 GPa stress. A model for the low-field electron mobility in strained-silicon has been proposed in [9]. It describes the mobility tensor in strained-silicon layers as a function of the strain. The model includes the effect of strain-induced splitting of the conduction band valleys in silicon, intervalley scattering, doping dependence, and temperature dependence.

We present a systematic study of the electron high-field transport in silicon under biaxial and uniaxial stress conditions using full-band Monte Carlo (MC) simulations. A strain dependent empirical model describing the velocity vector as a function of the magnitude and direction of the electric field is presented. The goal of this work is an analytical description of the velocity field characteristics at high electric field. To obtain a complete mobility model for device simulation, this high-field behavior has to be combined with mobility models incorporating the effects dominant at low driving field, such as impurity scattering and surface roughness scattering. This approach, sometimes referred to as the onion model, starts with a proper expression for the lattice mobility, and adds then the effects of impurity scattering, surface scattering, and finally velocity saturation. Using this notion, the presented high-field model can be combined with any low-field model incorporating the aforementioned scattering effects. Note that effects such as surface scattering and velocity saturation are dominant in different device regions. Surface roughness scattering is most effective for carriers confined in a channel, where the driving field is low. On the other hand, high driving fields occur in the pinch-off region, where carriers are no longer quantized in subbands, but behave bulk like. Indeed, the transition region of moderate driving fields, where a significant fraction of carriers is still quantized and already moderate carrier heating takes place, the error of this onion-type model may be somewhat higher than in the low-field and high-field limits.

II. High-Field Electron Transport in Strained Silicon

The velocity-field characteristics needed for the development of the analytical model have been obtained by full-band MC simulations using Vienna Monte Carlo (VMC) [10]. The MC simulator VMC [10], including full-band and analytical band models, allows the simulation of carrier transport in strained-silicon on SiGe with recent extensions considering strain effects

Manuscript received July 25, 2006. This work was supported by the European Commission NoE SINANO under Grant IST-506844, and D-DOTFET under Project 012150-2. The review of this paper was arranged by Editor C. McAndrew.

The authors are with Institut für Mikroelektronik, Technische Universität Wien, A-1040 Vienna, Austria (e-mail: dhar@iue.tuwien.ac.at).

Digital Object Identifier 10.1109/TED.2006.885639

0018-9383/$20.00 © 2006 IEEE

TABLE I
COUPLING CONSTANTS FOR INTERVALLEY SCATTERING IN SILICON IN $[10^8$ eV/cm$]$

Type of Scattering	g_1	g_2	g_3	f_1	f_2	f_3
Values	0.4716	0.7574	10.42	0.348	2.32	2.32

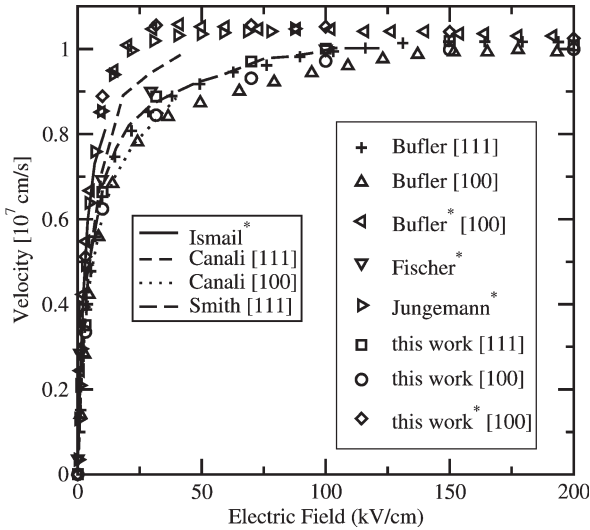

Fig. 1. Comparison of electron velocity versus field characteristics in unstrained and strained ($\star$) Si on $Si_{0.7}Ge_{0.3}$ for [100]/[111] field directions.

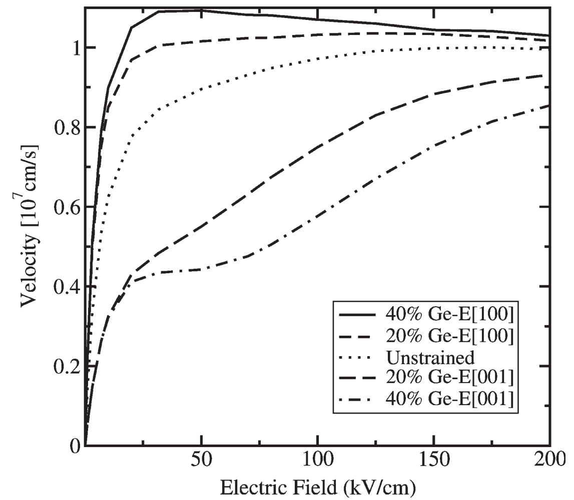

Fig. 2. Electron velocity in strained-silicon on SiGe with Ge content as a parameter for field along [100] and [001] directions.

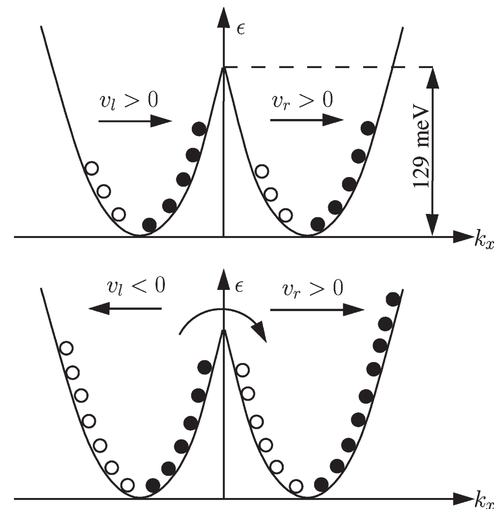

Fig. 3. Asymmetric electron populations of the double valley close to the equilibrium state (top) and at high field (bottom). Solid circles indicate electrons with positive group velocity (right side of each valley). Open circles refer to electrons with negative group velocity (left side of each valley).

arising from uniaxial stress along arbitrary directions. In this section, some peculiarities of the velocity-field characteristics in strained-silicon are discussed.

The band structure for strained-silicon was calculated using the empirical pseudopotential method [11]. Full-band MC simulations have been performed and the results calibrated with the existing theoretical and experimental data. It has been previously reported that the enhancement of the bulk low-field electron mobility saturates at around 1.7 [9]. In order to maintain the desired mobility enhancement, the g-type coupling constants had to be decreased by 6% and the f-type coupling constant increased by 16%, as compared to the original values proposed by Jacoboni [12]. The final values used are shown in Table I. In addition, it was required to adjust the acoustic deformation potential from its original value of 8.9 [13] to 8.5 eV. The effect of impact ionization has been neglected for the field regime investigated. Fig. 1 presents the velocity-field characteristics for unstrained and strained-silicon for different field directions as obtained from MC simulations. Also displayed are the results from Bufler *et al.* [14], Canali *et al.* [15], Smith *et al.* [16], Fischer and Hofmann [17], and Ismail *et al.* [18]. The simulation results agree well with measured data from Smith for the [111] field direction and with Canali for the [100] field direction for the unstrained case and with Jungemann and Meinerzhagen [13], Bufler, and Ismail for the strained case.

Fig. 2 depicts the velocity-field characteristics as obtained from MC simulations for biaxially strained-silicon grown on a relaxed SiGe substrate for different Ge content and field along the in-plane ([100]) and out-of-plane ([001]) direction, respectively. The total velocity increases with strain for a field along the [100] direction and it decreases for a field along the [001] direction. For the in-plane electric field ([100]) the electron velocity shows a region of small negative differential mobility. The velocity-field characteristics for field along [001] direction exhibit an untypical form for high strain levels. This phenomenon can be explained by the repopulation of valleys induced by the field.

For field along [001] direction the Δ_2 valleys are lowered in energy with increasing strain and have the longitudinal mass in the field direction. These valleys are located at a scaled distance of 0.85 and 1.15 from the center of the first Brillouin zone and are separated by an energy barrier of 129 meV at the X-point (Fig. 3). The average velocity in the left and right valley and also the average of these velocities are shown in Fig. 4. For low fields, electrons in both valleys are slightly displaced with respect to the valley minima. This results in the initial velocity increase for both valleys shown in Fig. 4. However, as the field increases, electrons in both valleys gain energy, and electrons from one valley can surpass the energy barrier and drift to the valley in the next Brillouin zone. As sketched in Fig. 3, there are

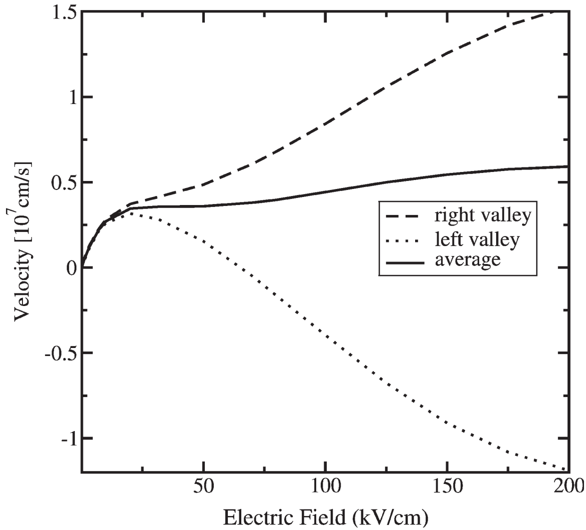

Fig. 4. Velocity versus field for left valley and right valley together with the average valley velocity, computed as explained in the text.

more electrons populating the right side of the double valley than the left side, giving rise to a slight increase in average velocity. If only the left valley is considered, there are more electrons populating the left edge of the single valley resulting in a negative valley velocity, as shown in Fig. 4.

III. Analytical High Field Velocity Model

In general, the high field mobility is modeled differently for the drift-diffusion and the hydrodynamic transport model. In the former case, mobility is modeled as a function of the driving force, whereas in the latter case a dependence on the carrier temperature is usually assumed. To describe nonlocal transport effects occurring in aggressively scaled devices a mobility model for the hydrodynamic framework would be desirable. Such a model could include a three-valley band structure and deal with arbitrary strain conditions. It would capture the essential physics of multivalley transport under a spatially rapidly varying electric field profile. However, one problem is complexity. A nonlinear system of nine unknowns, namely the valley populations, valley velocities, and valley temperatures, has to be solved numerically. The peculiar shape of the $v(E)$ curves for field along [001] direction would pose an additional problem, requiring some empirical fitting. The strain and carrier temperature dependence for each valley would require careful modeling in order to obtain realistic carrier temperatures and, consequently, realistic valley population. In the past, multivalley transport models have also been devised for compound semiconductors [19]. As a matter of fact, it seems that such multivalley transport models with separate carrier gases for each valley have never found application in commercial or academic device simulators.

To find a tradeoff between physical rigor and an acceptable level of model complexity we abstained from the multivalley approach and pursued a more empirical approach, where analytical expressions for the velocity-field characteristics are directly fitted to bulk MC data. Our model is restricted to such strain conditions where only one pair of X-valleys is shifted and four valleys remain degenerate. These conditions include biaxial stress and uniaxial stress applied along the $\{100\}$ axes of silicon. Another condition resulting in a separation of the Δ_2 and Δ_4 valleys is uniaxial stress in the $\{110\}$ direction. Depending on the stress applied, the strain tensor can be calculated using Hook's law and the strain-induced valley splitting can be obtained from linear deformation potential theory [20].

$$\Delta\varepsilon^{(i)} = \Xi_d(\varepsilon_{11} + \varepsilon_{22} + \varepsilon_{33}) + \Xi_u\varepsilon_{ii}, \qquad i = 1, 2, 3 \quad (1)$$

The values of the deformation potentials Ξ_d and Ξ_u have been identified as 1.1 and 9.29 eV, respectively. The value of Ξ_u has been extracted from the numerical band structure data. Equation (1) shows that the valley splitting depends only on the diagonal elements of the strain tensor. The proposed mobility model is thus applicable, if two diagonal elements are equal, $\epsilon_{11} = \epsilon_{22} \neq \epsilon_{33}$.

To develop a clear understanding of the model, we have to consider three different coordinate systems.

1) The principal coordinate system has to be oriented such that the unit vectors $\vec{e}_1$, $\vec{e}_2$, and $\vec{e}_3$ correspond to the [100], [010], and [001] crystallographic directions, respectively. In this system the Δ_4 valleys are aligned along the [100] and [010] directions, whereas the Δ_2 valleys are aligned along the [001] direction.
2) The unit vectors $\vec{e}_x$, $\vec{e}_y$, and $\vec{e}_z$ constitute the device coordinate system. In this system, the device geometry is defined. For performing device simulations it is essential to transform all transport parameters into this coordinate system.
3) A polar coordinate system is employed, comprising a unit vector along the field direction, $\vec{e}_E = \vec{E}/|E|$, and two orthogonal vectors $\vec{e}_\theta$ and $\vec{e}_\varphi$. The polar axis is aligned with the [001] direction. In terms of the polar angle θ and the in-plane (azimuth) angle φ, the unit vectors are defined as follows:

$$\vec{e}_E = \begin{pmatrix} \sin(\theta)\cos(\varphi) \\ \sin(\theta)\sin(\varphi) \\ \cos(\theta) \end{pmatrix}, \quad \vec{e}_\theta = \frac{\partial \vec{e}_E}{\partial \theta}, \quad \vec{e}_\varphi = \frac{1}{\sin(\theta)} \frac{\partial \vec{e}_E}{\partial \varphi}. \quad (2)$$

A. Parallel Velocity Model

A widely used model describing the electron high field behavior in unstrained-silicon has been adopted [21]:

$$v_E = \frac{2\mu_0 E}{1 + \left[1 + \left(\frac{2\mu_0 E}{v_s}\right)^\beta\right]^{1/\beta}}. \quad (3)$$

Here, μ_0 denotes the low field mobility and v_s the saturation velocity. The parameter β describes the transition from low to high fields. Although (3) can describe the high field behavior in unstrained-silicon, it can neither account for the small negative differential mobility nor the velocity plateau seen in strained-silicon (Fig. 2). We thus use an expression previously suggested

TABLE II
PARAMETER VALUES FOR THE PARALLEL VELOCITY COMPONENT v_E IN UNSTRAINED SILICON

Parameter	Units	E [100] E [001]	E [110] E [101]	E [$11\sqrt{2}$]
v_{s1}	[10^7 cm/s]	1.026	1.058	1.042
β_1	[1]	1.085	1.2475	1.273

in [22], which can handle all types of velocity-field characteristics resulting from the MC simulations performed:

$$v_E = \frac{2\mu_{\rm EE}E}{1+\left[1+\left(\frac{2\mu_{\rm EE}E}{v_s(1-\xi)}\right)^{\beta}\right]^{1/\beta}} + v_s\xi\frac{(E/\eta)^{\gamma}}{1+(E/\eta)^{\gamma}}. \quad (4)$$

Here, $\mu_{\rm EE}$ denotes the low-field mobility in the field direction, obtained by projection of the low-field mobility tensor as $\mu_{\rm EE} = \vec{e}_E^T \cdot \mu_0 \cdot \vec{e}_E$. $\vec{e}_E^T$ denotes the transpose of $\vec{e}_E$. The additional term incorporated in (4) models the velocity kink shown in Fig. 2. The relevance of the parameter ξ is twofold: It accounts for the velocity plateau occurring approximately at $v_s(1-\xi)$ and also signifies the small negative differential mobility occurring in strained-silicon for higher strain levels. The parameters η and γ are fit parameters.

All parameters depend on the strain-induced valley splitting, $\Delta\varepsilon = \varepsilon(\Delta_2) - \varepsilon(\Delta_4)$. The following empirical expressions were assumed

$$v_s = v_{s1} + v_{s2}\cdot\Delta\varepsilon \quad (5)$$

$$\beta = \beta_1 + \beta_2\cdot\Delta\varepsilon \quad (6)$$

$$\eta = \eta_1 + \eta_2\cdot\Delta\varepsilon \quad (7)$$

$$\gamma = \gamma_1 + \gamma_2\cdot\Delta\varepsilon \quad (8)$$

$$\xi = \frac{(\Delta\varepsilon/\xi_1)}{1+(\Delta\varepsilon\cdot\xi_2/\xi_1)^2}. \quad (9)$$

For all parameters except ξ, a linear dependence was found to be sufficient. The parameter ξ was modeled by the rational expression in (9). The parameters v_{si}, β_i, η_i, γ_i, ξ_i where $i = 1, 2$, are constants for a particular field direction. We have chosen the three high symmetry directions [100], [110], and [001], and two additional directions [101] and [$11\sqrt{2}$]. These five sample directions form a spherical triangle on a unit sphere. The parameters in (5)–(9) have been obtained using the optimization framework of MATLAB [23]. A multidimensional unconstrained nonlinear minimization (Nelder–Mead) technique was adopted for obtaining the parameter set. The optimized values of the parameters for these field directions are listed in Tables II–IV. It should be noted that the optimization technique is sensitive to the initial conditions of the parameters and therefore a small variation in the initial conditions can result in a slightly varied parameter set.

Fig. 5 shows the $v_E(E)$ characteristics for a 1 GPa stressed (along [001]) silicon layer for field along [100] and [001] directions, respectively. Application of uniaxial compressive stress enhances the velocity along [100] direction in the same way as biaxial tensile strain does. Conversely, applying uniaxial tensile stress results in an enhanced velocity along [001] direction.

B. Perpendicular Velocity Model

For the cases where the field is not oriented in a high symmetry direction, it is observed that an electron velocity perpendicular to the field direction develops. Fig. 6 shows the perpendicular electron velocity, $\vec{v}_\theta$ for field along the [101] direction for increasing stress level, as obtained from MC simulations. The component $\vec{v}_\theta$, although small for low stress levels, has a significant magnitude for intermediate field regimes and can result in a total velocity different from the parallel velocity. For symmetry reasons, the velocity component in the $\vec{e}_\varphi$ direction vanishes for all five sample directions.

The perpendicular velocity component vanishes for fields along the [100], [110], and [001] directions. For the field directions [101] and [$11\sqrt{2}$], the normal velocity can be expressed in terms of v_E and v_3

$$v_\theta = v_E - \sqrt{2}v_3. \quad (10)$$

After fitting v_E, the component v_3 is fitted using an expression similar to (4)

$$v_3 = \frac{\sqrt{2}\mu_{33}E}{1+\left[1+\left(\frac{2\mu_{33}E}{v_s(1-\xi)}\right)^{\beta}\right]^{1/\beta}} + \frac{v_s}{\sqrt{2}}\xi\frac{(E/\eta)^{\gamma}}{1+(E/\eta)^{\gamma}}. \quad (11)$$

To ensure the correct low-field behavior, $v_3 = \mu_{33}E_3$, the magnitude of the electric field E in the first term in (4) has to be replaced by $E_3 = E/\sqrt{2}$ to obtain (11). The correct high-field limit is introduced by replacing v_s in (4) by $v_{3,s} = v_s/\sqrt{2}$. For the unstrained case the values of the parameters β and v_s are identical with those listed in Table II. The fitting of the parameters in (11) is performed such that the error in v_θ is minimized. The values of the other parameter for the field directions [101] and [$11\sqrt{2}$] are listed in Table V.

C. Total Velocity for Fixed Field Direction

The total electron velocity vector is obtained by addition of the two components

$$\vec{v}_t = v_E\vec{e}_E + v_\theta\vec{e}_\theta \quad (12)$$

where $\vec{e}_E$ and $\vec{e}_\theta$ are the unit vectors parallel and perpendicular to the field direction. Fig. 7 shows a comparison of the velocity components and total velocity for -1 GPa stress for field along the [$11\sqrt{2}$] direction, as obtained from MC simulations and the analytical model. The results from the model for the sample field direction chosen are in good agreement with the MC data and demonstrate the validity of the model.

TABLE III
PARAMETER VALUES FOR THE PARALLEL VELOCITY COMPONENT v_E FOR $\Delta\epsilon < 0$

Parameter	Units	E [100]	E [001]	E[110]	E [101]	E [11$\sqrt{2}$]
v_{s2}	[10^5 cms^{-1}eV^{-1}]	-5.5691	33.731	1.4988	11.739	11.067
β_2	[eV^{-1}]	-0.33235	-5.2879	0.22885	-0.30235	-0.39907
ξ_1	[eV]	0.37994	-0.22859	0.45615	-0.84676	-0.76303
ξ_2	[1]	1.6239	1.0333	1.5468	6.3401	4.7611
η_1	[10^4 Vcm^{-1}]	2.1254	6.3369	0.6651	4.2133	5.4664
η_2	[10^5 Vcm^{-1}eV^{-1}]	-1.13	-2.748	-0.86273	-2.0402	-1.5317
γ_1	[1]	1.3707	2.6051	1.3869	2.4453	3.4612
γ_2	[eV^{-1}]	-0.73185	-6.3392	0.61215	-13.938	-7.1773

TABLE IV
PARAMETER VALUES FOR THE PARALLEL VELOCITY COMPONENT v_E FOR $\Delta\epsilon > 0$

Parameter	Units	E [100]	E [001]	E [110]	E [101]	E [11$\sqrt{2}$]
v_{s2}	[10^5 cms^{-1}eV^{-1}]	-20.608	10.822	-14.625	2.2239	3.5825
β_2	[eV^{-1}]	0.472	0.5135	0.21785	-0.41762	-0.27011
ξ_1	[eV]	0.47701	-0.29814	1.0876	-1.3718	1.9381
ξ_2	[1]	3.1569	2.1639	-8.5962	-4.2752	5.5323
η_1	[10^4 Vcm^{-1}]	7.6075	3.7613	5.8913	0.25071	1.1382
η_2	[10^5 Vcm^{-1}eV^{-1}]	1.471	2.7214	1.3928	0.92226	-0.19962
γ_1	[1]	3.815	1.163	4.7754	1.4471	0.7351
γ_2	[eV^{-1}]	2.9118	4.8595	5.2425	0.14618	5.2995

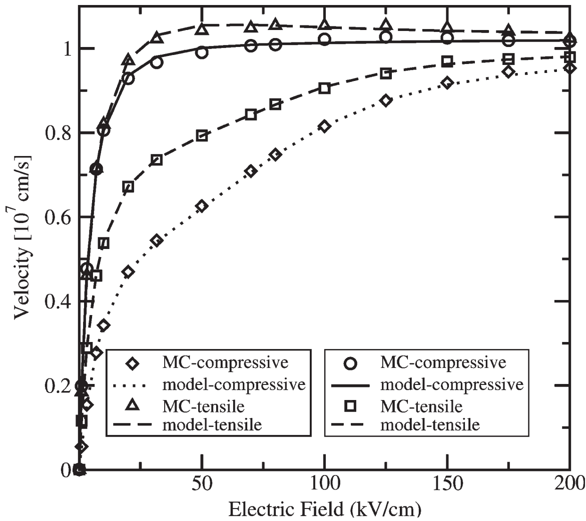

Fig. 5. Parallel electron velocity component versus field for silicon under uniaxial stress (1 GPa) along [001] and field along [100] (right legend) and [001] (left legend) directions, respectively.

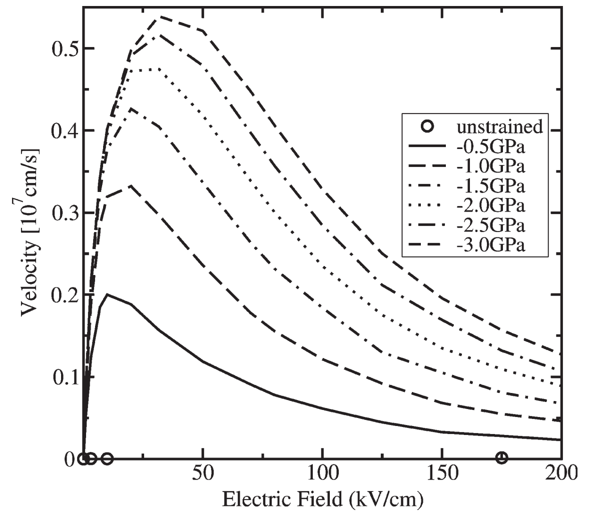

Fig. 6. Perpendicular velocity versus field for silicon under increasing uniaxial stress along [001] and field along [101].

D. Total Velocity for Arbitrary Field Direction

The velocity-field characteristics can be extended to other field directions using a spherical harmonics interpolation.

$$\Phi(\theta,\varphi) = \sum_{l=0}^{\infty}\sum_{m=0}^{l} a_{lm} P_l^m\left[\cos(\theta)\right]\cos(m\varphi). \quad (13)$$

Here, Φ is the function to be interpolated, a_{lm} denote the expansion coefficients and P_l^m are the associated Legendre polynomials. From the symmetry properties $\Phi(\theta,\varphi+\pi/2) = \Phi(\theta,\varphi)$ and $\Phi(\theta+\pi,\varphi) = \Phi(\theta,\varphi)$ it follows that l must be even and $m = 4n$. Truncating (13) after the fourth order yields

$$\Phi(\theta,\varphi) = a_{00}P_0^0(\chi) + a_{20}P_2^0(\chi) + a_{40}P_4^0(\chi) + a_{44}P_4^4(\chi)\cos(4\varphi) \quad (14)$$

TABLE V
PARAMETER VALUES FOR THE [001] VELOCITY COMPONENT v_3

Parameter	Units	E [101] $\Delta\epsilon < 0$	E [101] $\Delta\epsilon > 0$	E $[11\sqrt{2}]$ $\Delta\epsilon < 0$	E $[11\sqrt{2}]$ $\Delta\epsilon > 0$
v_{s2}	$[10^6\ \mathrm{cms}^{-1}\mathrm{eV}^{-1}]$	4.0975	2.8429	3.53	3.4858
β_2	$[\mathrm{eV}^{-1}]$	-1.7085	-0.22173	-1.7571	-0.26191
ξ_1	[eV]	-0.16917	-0.3354	-0.17293	-0.36817
ξ_2	[1]	0.75896	-1.9529	0.76209	2.2891
η_1	$[10^4\ \mathrm{Vcm}^{-1}]$	3.9982	5.9335	4.223	6.5366
η_2	$[10^5\ \mathrm{Vcm}^{-1}\mathrm{eV}^{-1}]$	-2.2147	1.9583	-2.1683	1.8587
γ_1	[1]	1.8204	1.9209	2.0921	1.668
γ_2	$[\mathrm{eV}^{-1}]$	-4.6684	3.5664	-3.5816	5.4713

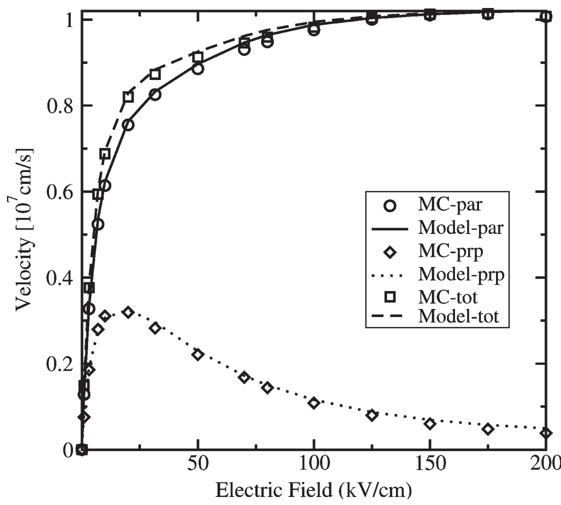

Fig. 7. Parallel (par) and perpendicular (prp) velocity components and total (tot) velocity versus field for silicon under uniaxial stress (−1 GPa) along [001] and field along $[11\sqrt{2}]$.

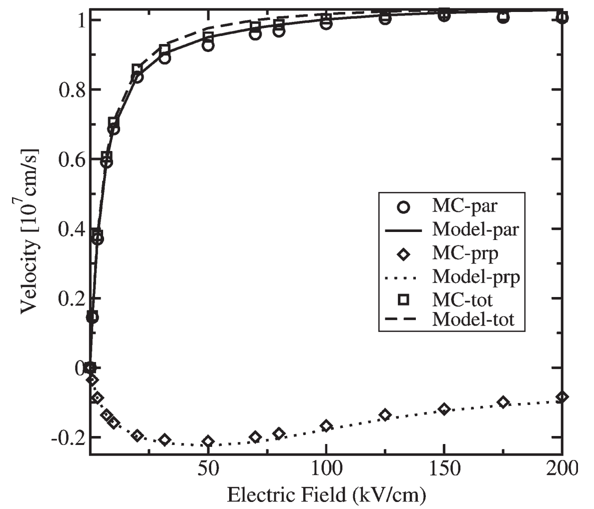

Fig. 8. Interpolated parallel (par) and perpendicular (prp) velocity components and the total (tot) velocity versus field for silicon under uniaxial stress (3 GPa) along [001] and field along [111].

where $\chi = \cos(\theta)$. Evaluating (14) for field directions [100], [110], [001], [101], and $[11\sqrt{2}]$ gives

$$\Phi_{100} = a_{00} - \frac{1}{2}a_{20} + \frac{3}{8}a_{40} + 105a_{44} \tag{15}$$

$$\Phi_{110} = a_{00} - \frac{1}{2}a_{20} + \frac{3}{8}a_{40} - 105a_{44} \tag{16}$$

$$\Phi_{001} = a_{00} + a_{20} + a_{40} \tag{17}$$

$$\Phi_{011} = a_{00} + \frac{1}{4}a_{20} - \frac{13}{32}a_{40} + \frac{105}{4}a_{44} \tag{18}$$

$$\Phi_{11\sqrt{2}} = a_{00} + \frac{1}{4}a_{20} - \frac{13}{32}a_{40} - \frac{105}{4}a_{44}. \tag{19}$$

To determine the four coefficients from the overdetermined system (15)–(19), we solve (15)–(17) exactly and minimize the error in (18) and (19)

$$a_{00} = \frac{1}{3}(\Phi_{100} + \Phi_{110} + \Phi_{001}) - \frac{7}{12}a_{40} \tag{20}$$

$$a_{20} = \frac{1}{3}(2\Phi_{001} - \Phi_{100} - \Phi_{110}) - \frac{5}{12}a_{40} \tag{21}$$

$$a_{40} = \frac{8}{35}(\Phi_{100} + \Phi_{110} + 2\Phi_{001} - 2\Phi_{011} - 2\Phi_{11\sqrt{2}}) \tag{22}$$

$$a_{44} = \frac{1}{210}(\Phi_{100} - \Phi_{110}). \tag{23}$$

It was found that interpolation of the quantities $\Phi = v_E^2$ and $\Phi = v_3^2$ gives good agreement to MC data. Fig. 8 show a comparison of the velocity components and the total velocity as obtained from the interpolation and MC simulations for field along the [111] direction for uniaxial tensile stressed silicon. It can be seen that tensile stress causes the parallel and perpendicular velocities to have opposite signs.

E. Simplification to Two-Dimensional Simulation Domains

For two-dimensional simulation domains, a simpler interpolation method can be used. In the following, we consider the case that $\vec{e}_3$ lies in the simulation domain, such that φ is fixed and only the variation of θ has to be considered. An alternative case would be a uniaxial stress orthogonal to the simulation domain, for example, in the width direction of a MOSFET. Then, $\theta = \pi/2$ and φ varies.

In the first case, the quantity Φ can be interpolated using the following polynomial

$$\Phi(\theta) = b_0 + b_2 \cos^2(\theta) + b_4 \cos^4(\theta). \quad (24)$$

Considering the special case of transport in the $\langle 010 \rangle$ plane ($\varphi = 0$), we can write the equation system

$$\Phi_{100} = b_0 \quad (25)$$

$$\Phi_{101} = b_0 + \frac{b_2}{2} + \frac{b_4}{4} \quad (26)$$

$$\Phi_{001} = b_0 + b_2 + b_4 \quad (27)$$

which gives the coefficients

$$b_2 = -3\Phi_{100} + 4\Phi_{101} - \Phi_{001} \quad (28)$$

$$b_4 = 2\Phi_{100} - 4\Phi_{101} + 2\Phi_{001}. \quad (29)$$

Similarly, for transport in a $\langle \bar{1}10 \rangle$ plane ($\varphi = \pi/4$), we have

$$\Phi_{110} = b_0 \quad (30)$$

$$\Phi_{11\sqrt{2}} = b_0 + \frac{b_2}{2} + \frac{b_4}{4} \quad (31)$$

$$\Phi_{001} = b_0 + b_2 + b_4 \quad (32)$$

giving

$$b_2 = -3\Phi_{110} + 4\Phi_{11\sqrt{2}} - \Phi_{001} \quad (33)$$

$$b_4 = 2\Phi_{110} - 4\Phi_{11\sqrt{2}} + 2\Phi_{001}. \quad (34)$$

The quantities to be interpolated are $\Phi = v_E^2$ and $\Phi = v_3^2$. Note that for a field in [100] and [110] direction, the component v_3 vanishes. Therefore, for this quantity the calculation of the coefficients simplifies because $\Phi_{100} = \Phi_{110} = 0$. Using the relations (28) and (29) for the $\varphi = 0$ plane and (33) and (34) for the $\varphi = \pi/4$ plane, the velocity components can be interpolated.

IV. Implementation Issues

The present model has been derived for a uniform electric field $\vec{E}$. To apply it in a drift diffusion-based device simulator, the electric field in the model has to be replaced by an appropriately defined driving force $\vec{F}_n$. Typical definitions of the driving force employed in practical devices simulators are the electric field component along the current density vector or the gradient of the quasi-Fermi level.

For the two-dimensional cases described in Section III-E, only one angle has to be determined. With the constant, two-dimensional vector $\vec{e}_3$ denoting the [001] direction, one obtains for the polar angle

$$\cos^2(\theta) = \frac{(\vec{F}_n \cdot \vec{e}_3)^2}{\vec{F}_n \cdot \vec{F}_n}. \quad (35)$$

The involved vectors are two-dimensional and specified in the device coordinate system.

The task of finding a tensor $\hat{\mu}$ that relates two given vectors $\vec{F}_n$ and $\vec{v}$ by $\vec{v} = \hat{\mu}\vec{F}_n$ has no unique solution. In two dimensions, this vector equation denotes two scalar equations, whereas the 2 by 2 matrix $\hat{\mu}$ has four unknown elements. The straightforward assumption of a diagonal matrix with diagonal elements $\mu_{xx} = v_x/F_{n,x}$ and $\mu_{yy} = v_y/F_{n,y}$ cannot be made, because this definition becomes singular whenever the driving force vector is parallel to the x or y axes.

To solve this problem one can probe the velocity vector for a second driving force vector. Using Cartesian coordinates, a vector orthogonal to $\vec{F}_n = (F_{n,x}, F_{n,y})$ can be easily found as $\vec{G}_n = (-F_{n,y}, F_{n,x})$. The four matrix elements can now be uniquely determined from the following two vector equations

$$\vec{v}_t(\vec{F}_n) = \hat{\mu}\vec{F}_n \quad (36)$$

$$\vec{v}_t(\vec{G}_n) = \hat{\mu}\vec{G}_n. \quad (37)$$

Implementation of a full tensorial mobility model in two dimensions would require the following quantities. We consider some edge α of an unstructured mesh, connecting the nodes i and j. The unit vector along this edge is given by $\vec{e}_\alpha = (\vec{r}_j - \vec{r}_i)/|\vec{r}_j - \vec{r}_i|$. A vector $\vec{e}_\beta$ orthogonal to $\vec{e}_\alpha = (\alpha_x, \alpha_y)$ can be defined as $\vec{e}_\beta = (-\alpha_y, \alpha_x)$. The box integration method requires the projection of the current density onto the edge, $j_\alpha = \vec{j} \cdot \vec{e}_\alpha$. For a mobility tensor with nonzero off-diagonal elements this current component becomes

$$j_\alpha = q n_\alpha (\mu_{\alpha\alpha} F_\alpha + \mu_{\alpha\beta} F_\beta) \quad (38)$$

where n_α denotes the carrier concentration at the mid point edge α. This equation states that the current component along the edge is driven not only by the driving force component along the edge, F_α, but also by the perpendicular component F_β. The Scharfetter–Gummel scheme [24] gives a discrete representation of the component F_α as a function of the variables at nodes i and j. The perpendicular component F_β, however, cannot be determined from the variables at the two nodes. It can only be estimated by some kind of interpolation of the parallel components at neighboring edges. One possible extension of the Scharfetter–Gummel discretization has been proposed in [25].

V. Discussion

The high-field velocity model presented has been derived for bulk silicon. The model can consistently be used with the drift-diffusion transport model whenever the spatial variations of the potential are sufficiently smooth. However, even nowadays where gate lengths are in the decananometer regime, drift-diffusion-based simulations are still widely used to estimate transistor performance, despite the fact that this model cannot capture the strong nonlocal transport effects. The latter are usually accommodated by changing parameters, in particular by considerably increasing the saturation velocity. Also, the high-field velocity model cannot include nonlocal effects, as it is based on populations of the band minima being functions of the local electric field. One should be aware that extending the local drift-diffusion equation with a local high-field velocity model

cannot extend the limitation with respect to strongly nonlocal transport occurring in relevant technologies. Upscaling the velocity by some technology-dependent parameter may still add some physics to the model, as a rough estimate of the direction-dependence of high-field transport.

VI. SUMMARY

A comprehensive study of the electron high-field transport in strained-silicon for different field directions and stress conditions has been performed using full-band MC simulations. A phenomenological approach to calculate the mobility tensor at high electric fields has been proposed. The structure of the proposed high-field model can be summarized as follows.

1) For five given field directions the parallel components $v_E(E)$ of the velocity vectors are empirically fitted. These five chosen directions form a spherical triangle.
2) For two out of the five field directions a normal velocity component develops. The normal components $v_\theta(E)$ in the direction $\vec{e}_\theta$ are also empirically fitted. For all field directions chosen, the normal component along the $\vec{e}_\varphi$ direction will vanish.
3) The velocity vector for the actual field direction is obtained from the velocity vectors for the sample directions by means of interpolation.
4) In the crystallographic system, the mobility tensor is assumed to be diagonal. The three diagonal elements are determined from the velocity and field vectors.
5) The mobility tensor is transformed to the device coordinate system by a unitary transformation.

This approach seems to be more suitable for device simulation purpose than a more physics-based model due to the inherent complexities discussed in Section III. The presented model is applicable for all stress conditions which cause the X-valleys to split into twofold degenerate Δ_2 valleys and four-fold degenerate Δ_4 valleys. It has been extended to arbitrary field directions using an interpolation technique. The path of implementing the model in drift-diffusion-based device simulator is briefly outlined.

REFERENCES

[1] K. Uchida, R. Zednik, C. Lu, H. Jagannathan, J. McVittie, P. McIntyre, and Y. Nishi, "Experimental study of biaxial and uniaxial strain effects on carrier mobility in bulk and ultrathin-body SOI MOSFETs," in *IEDM Tech. Dig.*, 2004, pp. 229–232.

[2] A. Shimizu *et al.*, "Local mechanical-stress control (LMC) : A new technique for CMOS performance enhancement," in *IEDM Tech. Dig.*, 2001, pp. 433–436.

[3] J. Welser, J. Hoyt, and J. Gibbons, "NMOS and PMOS transistors fabricated in strained-silicon/relaxed silicon-germanium structures," in *IEDM Tech. Dig.*, 1992, pp. 1000–1002.

[4] K. Rim, J.-L. Hoyt, and J.-F. Gibbons, "Transconductance enhancement in deep submicron strained Si N-MOSFETs," in *IEDM Tech. Dig.*, 1998, pp. 707–710.

[5] J.-L. Hoyt *et al.*, "Strained-silicon MOSFET technology," in *IEDM Tech. Dig.*, 2002, pp. 23–26.

[6] A. Lochtefeld and D. Antoniadis, "Investigating the relationship between electron mobility and velocity in deeply scaled NMOS via mechanical stress," *IEEE Electron Device Lett.*, vol. 22, no. 12, pp. 591–593, Dec. 2001.

[7] S. Maikap, C. Yu, S. Jan, M. Lee, and C. Liu, "Mechanically strained Si NMOSFETs," *IEEE Electron Device Lett.*, vol. 25, no. 1, pp. 40–42, Jan. 2004.

[8] S. Ito *et al.*, "Mechanical stress effect of etch-stop nitride and its impact on deep submicron transistor design," in *IEDM Tech. Dig.*, 2000, pp. 247–250.

[9] S. Dhar, H. Kosina, V. Palankovski, E. Ungersboeck, and S. Selberherr, "Electron mobility model for strained-Si devices," *IEEE Trans. Electron Devices*, vol. 52, no. 4, pp. 527–533, Apr. 2005.

[10] *VMC 2.0 User's Guide*, Institut für Mikroelektronik, Technische Universität Wien, Wien, Austria, 2006. [Online]. Available: http://www.iue.tuwien.ac.at/software

[11] M. Rieger and P. Vogl, "Electronic-band parameters in strained $\mathrm{Si}_{1-x}\mathrm{Ge}_x$ Alloys on $\mathrm{Si}_{1-y}\mathrm{Ge}_y$ substrates," *Phys. Rev. B, Condens. Matter*, vol. 48, no. 19, pp. 14 276–14 287, Nov. 1993.

[12] C. Jacoboni and L. Reggiani, "The Monte Carlo method for the solution of charge transport in semiconductors with applications to covalent materials," *Rev. Mod. Phys.*, vol. 55, no. 3, pp. 645–705, Jul. 1983.

[13] C. Jungemann and B. Meinerzhagen, *Hierarchical Device Simulation—The Monte Carlo Perspective*. New York: Springer-Verlag, 2003.

[14] F. Bufler, P. Graf, S. Keith, and B. Meinerzhagen, "Full band Monte Carlo investigation of electron transport in strained Si grown on $\mathrm{Si}_{1-x}\mathrm{Ge}_x$ substrates," *Appl. Phys. Lett.*, vol. 70, no. 16, pp. 2144–2146, Apr. 1997.

[15] C. Canali, G. Ottaviani, and A. Alberigi-Quaranta, "Drift velocity of electrons and holes and associated anisotropic effects in Si," *J. Phys. Chem. Solids*, vol. 32, no. 8, pp. 1707–1720, 1971.

[16] P. Smith, M. Inoue, and J. Frey, "Electron velocity in Si and GaAs at very high electric fields," *Appl. Phys. Lett.*, vol. 37, no. 9, pp. 797–798, Nov. 1980.

[17] B. Fischer and K. Hofmann, "Full band Monte Carlo model for electron and hole transport in strained Si including inelastic acoustic phonon scattering," *Appl. Phys. Lett.*, vol. 74, no. 15, pp. 2185–2187, Apr. 1999.

[18] K. Ismail, S. Nelson, J. Chu, and B. Meyerson, "Electron transport properties of Si/SiGe heterostructures: Measurements and device applications," *Appl. Phys. Lett.*, vol. 63, no. 5, pp. 660–662, Aug. 1993.

[19] W. Hänsch, *The Drift Diffusion Equation and its Application in MOSFET Modeling*. New York: Springer-Verlag, 1991.

[20] I. Balslev, "Influence of uniaxial stress on the indirect absorption edge in silicon and germanium," *Phys. Rev.*, vol. 143, no. 2, pp. 636–647, Mar. 1966.

[21] *MINIMOS-NT 2.1 User's Guide*, Technische Universität Wien, Wien, Austria, 2004.

[22] S. Dhar, G. Karlowatz, E. Ungersboeck, and H. Kosina, "Numerical and analytical modeling of the high-field electron mobility in strained Si," in *Proc. SISPAD*, 2005, pp. 223–226.

[23] *MATLAB—Language of Technical Computing, User's Guide, Release 14.0*, MathWorks, Inc., Natick, MA, 2004. [Online]. Available: http://www.mathworks.com/

[24] D. L. Scharfetter and H. K. Gummel, "Large signal analysis of a silicon read diode oscillator," *IEEE Trans. Electron Devices*, vol. ED-16, no. 1, pp. 64–77, Jan. 1969.

[25] J. Egley and D. Chidambarao, "Strain effects on device characteristics: Implementation in drift-diffusion simulators," *Solid State Electron.*, vol. 36, no. 12, pp. 1653–1664, Dec. 1993.

Siddhartha Dhar (S'06) was born in New Delhi, India, in 1979. He received the B.E. degree in electrical engineering from Delhi College of Engineering, Delhi, India, in 2001 and the M.Sc. degree in microelectronics and microsystems from Technical University of Hamburg, Harburg, Germany, in 2003. He is currently working toward the Ph.D. degree at Institut für Mikroelektronik, Vienna, Austria.

In April 2004, he joined the Institut für Mikroelektronik, Technische Universität Wien. His research interests include device modeling and simulation of strained-silicon CMOS transistors and circuit level simulation in general.

Hans Kosina (S'89–M'93) received the "Diplomingenieur" and Ph.D. degrees in electrical engineering, and the "venia docendi" in microelectronics, in 1987, 1992, and 1998, respectively, all from Technische Universität Wien, Vienna, Austria.

For one year, he was with Institute of Flexible Automation at the Technische Universität Wien, and joined then the Institut für Mikroelektronik, Vienna, Austria, where he is currently an Associate Professor. In summer 1993, he was a Visiting Scientist with Motorola, Inc., Austin, TX, and in summer 1999 a Visiting Faculty, Intel Corporation, Santa Clara, CA. His current research interests include device modeling of semiconductor devices, nanoelectronic devices, organic semiconductors and optoelectronic devices, development of novel Monte Carlo (MC) algorithms for classical and quantum transport problems, and computer-aided engineering in ultralarge scale integration technology.

Dr. Kosina has been an Associate Editor of the IEEE TRANSACTIONS ON COMPUTER-AIDED DESIGN OF CIRCUITS AND SYSTEMS since January 2004.

Gerhard Karlowatz was born in Mödling, Austria, in 1972. He received the degree of Diplomingenieur in physics from Technische Universität Wien, Vienna, Austria, in October 2003. He is currently working toward the Ph.D. degree at Institut für Mikroelektronik, Vienna, Austria.

In December 2003, he joined the Institut für Mikroelektronik. His scientific interests include MC simulation and modeling of optical devices.

Stephan Enzo Ungersboeck was born in Vienna, Austria, in 1977. He received the degree of Diplomingenieur in physics from Institut für Mikroelektronik, Vienna, Austria, in May 2002. He is currently working toward the Ph.D. degree at Technische Universität Wien, Vienna, Austria.

In June 2002, he joined the Technische Universität Wien. He held a visiting research position with Samsung Advanced Institute of Technology in Seoul, Korea, in summer 2003. His scientific interests include MC simulation, band structure calculations, simulation of carbon nanotubes, and quantum–mechanical confinement in submicrometer MOSFETs.

Tibor Grasser (SM'05) was born in Vienna, Austria, in 1970. He received the degree of "Diplomingenieur" in communications engineering, the Ph.D. degree in technical sciences, and the "venia docendi" in microelectronics, all from Institut für Mikroelektronik, Vienna, Austria, in 1995, 1999, and 2002, respectively.

In 1996, he worked with Institut für Mikroelektronik, Vienna, Austria, where he is currently employed as an Associate Professor. Since 1997, he has headed the MINIMOS-NT development group, working on the successor of the highly successful MINIMOS program. From October to December 1997, he was with Hitachi, Ltd., Tokyo, Japan, as a Visiting Research Engineer. In 2001, he was also a Visiting Researcher with Alpha Development Group, Compaq Computer Corporation, Shrewsbury, NJ. In 2003, he was appointed Head of the Christian Doppler Laboratory for technology computer-aided design in microelectronics, an industry-funded research group embedded in the Institut für Mikroelektronik. His current scientific interests include circuit and device simulation, device modeling, and reliability issues.

Siegfried Selberherr (M'79–SM'84–F'93) was born in Klosterneuburg, Austria, in 1955. He received the degree of "Diplomingenieur" in electrical engineering and the Ph.D. degree in technical sciences, both from Technische Universität Wien, Vienna, Austria, in 1978 and 1981, respectively.

He has been holding the "venia docendi" on computer-aided design since 1984. Since 1988, he has been the Chair Professor with Institut für Mikroelektronik, Vienna, Austria, and from 1999 to 2005 served as Dean of the Fakultät für Elektrotechnik und Informationstechnik at the Technische Universität Wien, Austria. His current research interests are modeling and simulation of problems for microelectronics engineering.